PUBLICATION [P1]

Experimental Analysis on Performance and Durability of SOFC Demonstration Unit

In: Fuel Cells 10 (3), pp. 440-452

ORIGINAL RESEARCH PAPER

Fuel Cells DOI: 10.1002/fuce.200900152

Experimental Analysis on Performance and Durability of SOFC Demonstration Unit

M. Halinen[1]*, J. Saarinen[1], M. Noponen[1a], I. C. Vinke[2], J. Kiviaho[1]

[1] VTT Technical Research Centre of Finland, Fuel Cells, P.O. Box 1000, Biologinkuja 5, Espoo, FI-02044 VTT, Finland
[2] Forschungszentrum Jülich GmbH, Institute of Energy Research -Fuel Cells (IEF-3), D-52425 Jülich, Germany

Received August 06, 2009; accepted December 02, 2009

Abstract

A technical description and experimental analysis of a SOFC demonstration unit is presented. The unit contains most of the primary BoP-components of a complete SOFC system, except of air and fuel recirculation equipment or fuel system compressor. Natural gas is used as the fuel and electricity is supplied to the electric grid. A 5 kW power class planar SOFC stack from Research Centre Jülich is assembled to the demo unit and a long-term experiment is conducted to assess the characteristic performance and durability of different components of the unit (e.g. the SOFC stack, the fuel pre-reformer and air heat exchangers). The evolution of absolute voltage drop of the stack over time is found to be of the same magnitude when compared to short stack experiments. Thus, other system components are not observed to cause an increase in the characteristic voltage drop of the stack. Two BoP-components, the afterburner and the power conversion unit failed to operate as designed. The performance of other BoP-components i.e. fuel pre-reformer and heat exchangers were satisfactory during the test run, and no significant performance loss could be measured.

Keywords: Balance of Plant, Durability, Experimental Results, Solid Oxide Fuel Cell, Stack, Voltage Degradation

1 Introduction

Solid oxide fuel cells (SOFCs) are considered an advantageous technology in energy production due to the high fuel conversion efficiency, modular design possibilities and fuel flexibility. High operating temperature makes SOFCs well suited for combined heat and power production (CHP) or for hybrid systems where the SOFC stack is coupled with a gas turbine. Fuel processor design is simplified compared to low temperature fuel cell types due to high operating temperature that enables direct oxidation of carbon monoxide and the use of hydrocarbon fuels *via* internal reforming reactions. The theoretical efficiency of the SOFC is not governed by size when compared to e.g. Carnot- or Rankine-cycle based energy production. Thus, SOFCs can be utilised for various applications with different power scale e.g. auxiliary power units for cars and trucks, residential and distributed CHP or stationary power production.

The widespread commercialisation of the SOFC technology is hindered by relatively higher cost of the SOFC systems when compared to the established technology for energy production e.g. engines or gas turbines. The price for both SOFC stacks along with other system components is high and the availability of products is poor due to the absence of developed markets and production. Along with the reduction of cost, long lifetime and high availability are prerequisites for a SOFC system for both stationary and micro CHP applications. The inherent voltage degradation phenomenon of the SOFC stacks is the most important factor that affects the durability and lifetime of a SOFC system. For stationary applications, voltage degradation rates below 0.25% kh^{-1} have to be achieved to ensure a long enough lifetime for the products [1, 2]. Currently, operating times for planar SOFC stacks that

[*] *Corresponding author, matias.halinen@vtt.fi*
[a] *Present affiliation: Wärtsilä, Product Centre Ecotech, Fuel Cells*

span up to and over 10,000 h with degradation rates below 1% kh^{-1} have been reported [3–5].

In addition to the SOFC stack, also the other components of the system, and the system as a whole, must endure years of continuous operation without unreasonable performance degradation or component failures. In the absence of large-scale production of dedicated components and peripherals for SOFC systems, the lifetime and performance of system components are not well established. Operation times of over thousands of hours for complete SOFC systems with a varying degree of availability have been achieved and reported [3, 6–9]. However, the level of reporting is typically very general and no information is given on the fundamental process parameters such as fuel and air utilisation, or current density during the operation of the system. Additionally, the effect of different system components on the performance and durability of the system as a whole is not assessed.

It can be argued that a more comprehensive understanding of issues related to the reliability and durability of SOFC systems is needed in order to attain similar operation times and degradation rates for complete SOFC systems when compared to the lifetime of individual stacks. Therefore, long-term experiments with complete SOFC systems are needed to measure and determine the effect of system components on the degradation and lifetime of SOFC stack. In this paper, the technical design and experimental analysis of a SOFC demonstration unit are presented. The unit was designed and constructed in a Finnish publicly funded SOFC research and development programme, which consisted of system and BoP-component development, system modelling and characterisation of SOFC cells and short stacks in system relevant operating conditions [10, 13, 20, 24]. The unit was constructed in order to demonstrate SOFC technology and assess the performance, durability and reliability of a complete grid connected SOFC system with natural gas as the fuel [10]. Moreover, the experimental results obtained with the unit could be used to develop and validate modelling tools for SOFC systems [11–13]. Results from a 7,000 h test run with a 5 kW power class stack are presented. Characteristic performance and durability of different system components e.g. fuel processing unit, heat exchangers, and the SOFC stack are reported.

2 Experimental

2.1 System Layout and the SOFC Stack

The demonstration unit included all the most important balance of plant components (BoP) of a SOFC system i.e. a planar stack, fuel pre-reformer unit, power conversion and grid interconnection equipment, heat exchangers for air and fuel, a catalytic burner, a blower for cathode air and mass flow controllers for other reactants, automation and control system, and purge gas containers for system shutdown and start-up situations (Figure 1).

The unit was constructed in order to demonstrate SOFC technology, assess the durability and reliability of SOFC stacks and BoP-components with long-term testing for several thousands of hours and to study the characteristic performance of different components and the interactions between the components. In order to obtain characteristic measurement data from individual components, a non-integrated design was applied. The intention with the non-integrated design was to reduce the effect of surface-to-surface heat transfer between components and to make modifications and

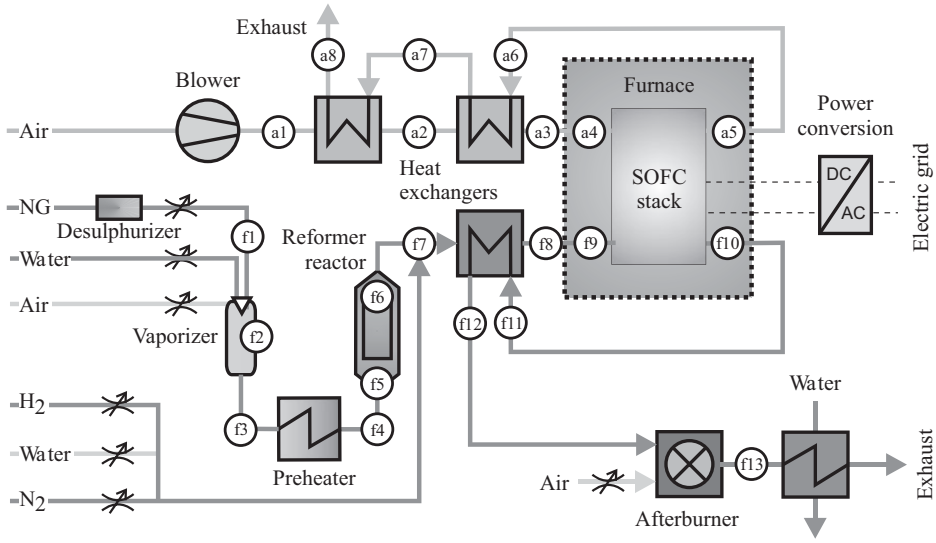

Fig. 1 Principle layout of the SOFC demonstration unit. Numbered circles represent measurement positions at the air and fuel systems of the unit.

replacements of different components easy. Thus, the unit was not designed to be thermally self-sufficient. Components and piping that operated above the room temperature were insulated with ceramic fibre insulation felts (isoTHERM S) and mineral wool sleeves. Additionally, the heat loss in the pipelines between the heat exchangers, the reformer unit and the stack was compensated with electric trace heating elements. Furthermore, it was necessary to position the SOFC stack in a furnace to make the assembly and curing of the stack possible on-site. The furnace was also used for start-up and to influence the temperature of the stack during system operation. Heating elements were used in the fuel system to vaporise the water and preheat the gas before the reformer reactor.

In order to collect relevant measurement information of the different components of the system, temperature and pressure were measured at several positions at the fuel and air systems. At the fuel system, temperature was measured at positions f2–f7 and f9–f13, and pressure at positions f1, f2, f7, f8, f11 and f12, depicted in Figure 1. At the air system, the temperature was measured at positions a1-a8 and the pressure at positions a1, a3, a6 and a8. Thermocouples (K-type, Class 1, ± 4 °C) were used for all temperature measurements. Pressure was measured with digital differential pressure meters (0–1,000 ± 3 mbarg, Keller PR-33).

The SOFC stack used in the unit was designed, manufactured and assembled by Forschungzentrum Jülich (FZJ) [14]. It utilised planar anode-supported cells with metallic interconnect plates made from CroFer22APU steel, which were coated with a MnOx/LCC10 contact layer at the air side. Glass-ceramic seals (Glass #76) were used to seal the stack. Fuel and air were distributed to cells in counter-flow pattern with internal manifold [15]. The 5 kW class stack used in the experiments consisted of 50 rectangular unit cells with an active area of 361 cm^2. The stack was resting on top of ceramic bricks inside the furnace. The inner dimensions of the furnace were 1,100 mm × 1,100 mm, the inner height was 640 mm and the thickness of the insulation layer was 150 mm. The heating elements of the furnace were situated on two opposite sides of the furnace. Current was collected from the end plates of the stack with steel bars that were led through the bottom of the furnace. Gas pipelines were, likewise, led through the bottom of the furnace.

The voltage was measured individually from all 50 unit cells in the stack with platinum wires that were spot-welded to the interconnect plates and end plates of the stack. The maximum error for the voltage measurements was ±9 mV. The flow-wise temperature profile was measured from interconnect plates situated above cells 3, 25 and 48, counting from the bottom of the stack. Thermocouples (K-type, Class 1) were used for the temperature measurements. The thermocouples were inserted inside 35 mm deep holes in the interconnect plates. In addition, the inlet and outlet temperatures of the fuel and air were measured from the pipeline ~10 cm from bottom plate of the stack (positions a4, a5, f9 and f10 in Figure 1).

2.2 Fuel System

The conventional nickel-cermet anode used in SOFCs is an effective steam-reforming catalyst, and therefore, able to convert hydrocarbons to hydrogen and carbon monoxide that can be utilised in electrochemical reactions. However, complete internal reforming can lead to local cooling at the fuel inlet area caused by a fast endothermic steam reforming reactions, and large temperature gradients can develop which may lead to cell cracking. Additionally, heating the fuel directly to operating temperature of the stack without pre-reforming of the fuel at lower temperatures increases the probability of hydrocarbon cracking and carbon formation in the heat exchangers or pipelines [16]. Without pre-reforming, some higher hydrocarbons can coke the nickel substrate at the anode electrode resulting in performance degradation and ultimately destruction of the cell [17, 18]. Due to the above-mentioned issues, prereforming of hydrocarbon fuels is usually necessary.

With natural gas, where the methane is the main constituent of the fuel, the degree of pre-reforming (*DoR*) of methane should be selected to optimise system-operating conditions. At nominal operating conditions, it is beneficial to maximise the amount of internal reforming reactions as the endothermic steam reforming of methane cools down the stack and decreases the need for surplus cathode air, which improves electrical efficiency [19]. At part-load and system stand-by situations, the amount of heat losses from the system is increased with respect to the heat produced by the stack. Therefore, in these situations, it may be beneficial to increase the *DoR* and limit the amount of methane fed into the stack [13]. As a result, the temperature and the voltage of the stack are increased, which can improve the system efficiency.

The reformer unit for natural gas used in the system could be operated at steam reforming conditions and, additionally, air could be supplied into the reactor to utilise exothermic partial oxidation reactions [20–22]. It consisted of mass flow controllers for natural gas (0–35.0 ± 0.5 l_N min^{-1}), water (0–80 ± 1 g min^{-1}) and air (0–60.0 ± 0.7 l_N min^{-1}), sulphur removal reactor, vaporiser, preheater, reactor chamber equipped with a proprietary monolithic catalyst (Süd-Chemie) and a heat exchanger before the stack. The natural gas used in Finland contains 4–10 ppm of sulphur containing THT odorant, and if not removed from the natural gas, it can deactivate the anode, lower the cell voltage and cause increased degradation [20]. The THT odourant was removed with an absorbent (Süd-Chemie) operating at room temperature. The adsorbent was changed on regular basis to keep the fuel supply free of sulphur. Concurrently, the impurities in the water supply were removed with ion-exchange resin. Natural gas and water were fed through a gas atomising nozzle into the vaporisation chamber. The supply pressure for natural gas and water was ~3 barg. Air was fed into the vaporisation chamber through a separate inlet. The reactor and the catalyst were not heated during operation. The heat used in the steam reforming reaction was provided by pre-

heating the inlet gases with electric heaters. Additionally, heat was supplied to the reactor by exothermic partial oxidation reactions when air was fed to the reformer unit. Temperature was measured at the reactor inlet, from the leading surface of the catalyst and at the reactor outlet (positions f4, f5 and f6 in Figure 1). Pressure was measured from the natural gas inlet before the gas atomising nozzle and from the vaporisation chamber (positions f1 and f2). A heat exchanger was situated between the reactor and the stack in order to increase the temperature of the fuel before the stack inlet. The heat exchanger was of a welded plate type and it was manufactured in-house. Temperature (positions f7, f8 and f11) and pressure (positions f7, f8, f10 and f11) were measured before and after the heat exchanger. Steel grade 1.4404 was used for the vaporiser and steel grade 1.4835 was used for all other components and piping at the fuel system of the demonstration unit.

Reformer exhaust gas was analysed with an online gas analyser (Sick S710 series) and with gas chromatographs (HP 6850A and HP 5890 Series II). The accuracy of the online analyser was further improved by calibrating it with varying gas mixture that correspond the different compositions of the exhaust gas. After calibration, the accuracy of the online analyser was ±0.5% for CO, CO_2 and CH_4 and ±1% for H_2. The composition of the exhaust gas on wet basis was calculated on the basis of carbon and nitrogen mass balances solved with the inlet mass flow measurements for air, water and natural gas and with exhaust gas analysis.

The unit could also be operated with gas mixture containing hydrogen (0–70.0 ± 0.8 l_N min^{-1}), nitrogen (0–70.0 ± 0.8 l_N min^{-1}) and steam (0–200 ± 2 gh^{-1}). Water was evaporated and mixed with gases by using a temperature-controlled evaporative mixer (Bronkhorst CEM-202). The gas mixture could be used to reduce the anode substrate after the stack assembly, as fuel during system operation and as purge gas during the heating and cooling of the unit to keep the anode substrate at reducing atmosphere.

Unused fuel in the anode exhaust gas was oxidised with air in a catalytic burner. The burner consisted of four successive segments equipped with cylindrical monolith catalysts. The burner and catalysts were manufactured in-house. Each catalyst segment had an individual air inlet. Air was supplied to the burner with a thermal mass flow controller (0–500 ± 6 l_N min^{-1}) and divided between the segments with rotameters. Downstream from the burner, the exhaust gas was fed through a water-cooled heat exchanger in order to retrieve the heat and condensate the water vapour before the exhaust.

2.3 Air System

Ambient air provides the source of oxygen, which is needed for electrochemical reactions at the cathode, and the air can be fed into the stack e.g. with air blowers. The use of over-stoichiometric amounts of air is necessary to dissipate the heat produced by the SOFC stack under electrical loading and prevent overheating of the stack to excessive operating temperatures. The inlet ambient air has to be preheated closer to the operating temperature of the stack to avoid local cooling of the stack at the air inlet, which could cause damaging temperature gradients or decrease the stack voltage under electric current by lowering the operating temperature [16]. The needed over-stoichiometric amount of air can vary between 3 and 10 (U_{AIR} between 0.10 and 0.33) depending on the *DoR* and the permissible temperature increase of air in the stack [19]. Such amounts of air lead to large air preheat duty and the energy needed for preheating must be recuperated from the stack's exhaust gases in order to achieve practical system efficiencies.

Ambient air was supplied to the unit with two-side channel blowers connected mechanically into series (Ventur SC-20C). Two blowers were used to reach pressures above 300 mbar. A filter was present at the blower inlet to remove particles from the air. Rotation speed of the blower was controlled with an inverter and the air flow was measured with a thermal mass flow metre (0–1,000 ± 20 l_N min^{-1}). Two heat exchangers for low and high temperature were connected in series in order to pre-heat inlet air to the stack. The design with two heat exchangers was chosen for the air system in order to reduce the temperature difference between the inlet and outlet and thus the thermal stresses induced to the heat exchangers. Concurrently, poor commercial availability of single heat exchanger that would meet the specified operating temperature necessitated this approach.

The low temperature heat exchanger was of a fully welded plate type (Raucell 120-23). Maximum operating temperature for this heat exchanger was designed to be below 450 °C. The high temperature heat exchanger was of a tube and shell type designed and manufactured in-house, and the maximum operating temperature was designed to be below 800 °C. Steel grades used in the construction of the heat exchangers were 1.4404 and 1.4835 for lower and higher operating temperature, respectively. Temperature was measured before, after and between the heat exchangers at cold and hot sides (positions a1, a2, a3, a6, a7 and a8 in Figure 1). Pressure was measured before and after the two heat exchangers at hot and cold sides (positions a1, a3, a6, and a8).

2.4 Power Conditioning Equipment and Automation System

Power conditioning equipment is needed in SOFC systems in order to increase the stack's DC voltage high enough to enable high efficiency DC power conversion to AC power and synchronisation with the electricity grid. Power conditioning and grid interconnection equipment consisted of DC–DC converters, regenerative inverter, LC-filter and transformer. DC–DC converters were used to increase the voltage of the SOFC stack to ~400 VDC required by the inverter. The inverter transmuted DC to 200 VAC. A LC-filter was used to compensate the possible current and voltage disturbance from the system to electric grid. Finally, a transformer was used to increase the voltage from 200 to 400 VAC. The power

conversion unit was manufactured from off-the-shelf components by Verteco Inc. Electric current from the stack to the power conversion unit was measured using a shunt resistor (Metrix Electronics) with a maximum error of ±0.7 A. Alternatively, the stack could be operated without the power conversion unit by dissipating the produced electricity with a DC load (Chroma 63203) e.g. during initial characterisation of the stacks with hydrogen as a fuel. The DC load was connected parallel to the stack with grid interconnection equipment. The maximum error for the current measurement of the DC load was ±1.2 A.

In order to provide the capability for long term testing in a safe and reliable way, the demonstration unit was designed to be capable of unmanned operation. This was made viable by constructing an automation and control system, which consisted of a standard industrial PLC (Schneider Premium Series) and a PC-based monitoring station. The PC-based monitoring station was used as a human-machine-interface and as a measurement database. During unmanned operation, several critical process measurements i.e. individual cell voltages, temperature of the inlet and outlet gases of the stack, supply pressure of the reactants, air blower or power conditioning faults, temperature of the reformer reactor and system-wide pressure measurements were used to monitor the safe operating conditions of the unit. If the critical process measurements deviated beyond predefined limits, the unit was brought to a stand-by state by disconnecting the stack from the electric grid and aborting the fuel feed to the unit. Air and safety gas containing 97% Ar and 3% H_2 were supplied from gas bottles to the respective sides of the unit to keep the anode at reducing and cathode at oxidising atmosphere. The gas flow through the system during emergency shutdown situations was set to be ~1 l_N min^{-1}.

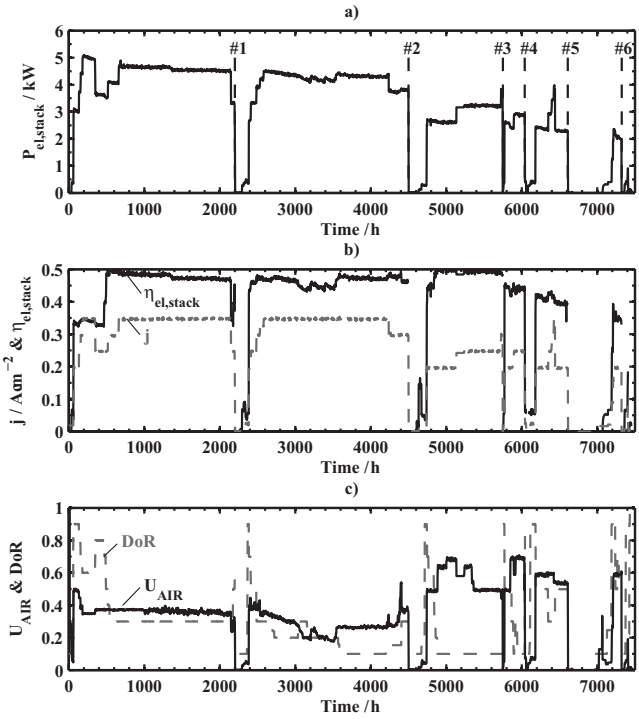

Fig. 2 Operating conditions of the demonstration unit and the electric power of the stack during the experiment. a) Gross electric power of the stack ($P_{el,stack}$). b) current density (j, dashed line) and gross electric efficiency ($\eta_{el,stack}$, solid line). c) Air utilisation (U_{AIR}, solid line) and degree of pre-reforming (*DoR*, dashed line). Shutdown situations are marked with numbers in the top figure.

3 Results and Discussion

3.1 Performance and Durability of the Stack

A long-term test run for a total period of 7,000 h was conducted with the demonstration unit, during which the stack was electrically loaded for over 6,000 h. During the experiment, the system was operated both at steady-state operating conditions, to assess the durability of the stack and BoP-components, and at varying operating conditions, to measure the characteristic operation of the unit components. The gross DC power ($P_{el,stack}$) of the stack along with the gross DC efficiency ($\eta_{el,stack}$), the current density, the air utilisation (U_{AIR}) and the degree of pre-reforming (*DoR*) of the fed methane (98% in natural gas) during the experiment are depicted in Figure 2. During the first 500 h of the experiment, fuel utilisation (U_{FUEL}) of the stack was 51%. During 500 to 4,500 h, U_{FUEL} was kept at 71% and the current density at 0.35 A cm^{-2} in order to measure the durability of the unit at nominal operating conditions. During this period, the $P_{el,stack}$ was between 4.5 and 5 kW and the $\eta_{el,stack}$ between 45 and 50%, depending on the operating parameters and duration of the experiment. After 4,500 h, the unit was used at lower current densities to measure the performance at part-load conditions at 0.2–0.25 A cm^{-2}, and also at lower operating temperature. Until 5,900 h, temperature of the furnace was kept at 780 °C during which $\eta_{el,stack}$ of 50% was achieved at part-load operating conditions. After 5,900 h, furnace temperature was decreased to 730 °C and a lower $\eta_{el,stack}$ of 40–45% was measured due to decreased stack voltage. At the end of the long term testing, at 7,000 h, the stack was insulated and the unit was operated without heating of the furnace in order to measure the effect of varying *DoR* to the temperature, voltage and effciency of the stack.

The demonstration unit and the stack could be operated over a wide range of operating conditions. During the experiment, the *DoR* varied between 0.1 and 0.9, U_{FUEL} between 0.51 and 0.71 and U_{AIR} between 0.17 and 0.68 when the cur-

rent density was at or above 0.2 A cm^{-2}. For the major part of the test, when the furnace was in use, varying the *DoR* did not result in significant changes in the temperature or voltage of stack, and the stack could be operated with *DoR* of 0.1 between 0.25 and 0.35 A cm^{-2}. At the end of the long term testing, when the furnace was not in use, a more pronounced effect of the *DoR* was observed, and *DoR* below 0.5 could not be achieved with 0.2 A cm^{-2}. This was due to the temperature smoothing effect of the furnace because of its high heat transfer area: the higher the temperature of the stack was with respect to the furnace temperature, the higher were the heat losses from the stack and vice versa. Therefore, the use of furnace affected the thermal balance of the stack to a great extent and provided an increased operability for the system, which would not have been possible without the furnace. It was observed that at low U_{AIR} values, the stack voltage decreased as the temperature of the stack was decreased due to increased air flow rate (Figure 2, 3,000–3,500 h). Interestingly, the operability of the stack was maintained at high U_{AIR} (above 0.33 [19]) values and no overheating of the stack occurred. This can be explained again by the use of furnace during the experiment.

As can be seen in Figure 2, the experiment was interrupted and the electric loading of the stack discontinued several times during the test run. Shutdown #1 at 2,200 h was initiated due to system servicing. The system was brought to a standby state and switched to hydrogen-nitrogen purge gas in order to clean the atomising nozzle of the fuel processor. The nozzle was clogged due to saturation of the ion-exchange resin, and the impurities present in the water deposited at the orifice of the nozzle. This induced a pressure drop increase over the nozzle (between f1 and f2), which would have eventually hindered the fuel and water flow to the fuel processing unit. As the ion-exchange mass was changed on a more regular basis based on the conductivity measurement of the water, clogging was not observed later during the experiment. Shutdown #2 at 4,500 h, occurred automatically due to supply failure of the natural gas and the system was brought to emergency shutdown. The fuel and air feeds were immediately discontinued and the unit was purged with a safety gas from gas bottles. Shutdowns #3 and #4 at 5,800 and 6,100 h, respectively, occurred automatically due to high pressure and low voltage alarms caused by partially frozen exhaust pipeline. The dew point of the anode exhaust gas after heat recovery and condensation was ~10 °C and the coincident outside temperature was –20 °C. As a result, the water vapour left in the exhaust gas froze in the exhaust pipeline obstructing the gas flow. The problem was solved by installing an electric trace heater to the exhaust pipeline.

After each of the above-mentioned shutdown situations, the individual cell voltages were compared at identical operating conditions with respect to current density, U_{FUEL}, U_{AIR}, *DoR* and furnace and stack temperature. The difference between individual cell voltages was at maximum ±20 mV before and after each shutdown, as some of the cells exhibited an increase in voltage. An exception to this was after the shutdown #3 at 5,800 h, where the flow of air purge gas was cut off for 3 h, due to exhaustion of purge air container, resulting in a significant loss of performance in cells number 1 and 7. With respect to these results, it can be concluded that the shutdown routines developed for the unit, if executed in a designed manner, along with a robust enough stack design, were sufficient to bring the system down safely without relevant decrease in the performance.

The shutdown #5 at 6,400 h was initiated to cool down the stack to room temperature to assemble insulation layer as the adjacent cells to cell #8 had already started to show progressive decrease in voltage after the shutdown at 5,800 h. The stack was then insulated with microporous insulation layer, heated back up to operating temperature mainly by pre-heating the inlet gases of the stack, and operated for another ~200 h. During this time, the effect of *DoR* on the temperature, voltage and efficiency of the stack was measured without external heating of the furnace. The final shutdown #6 at 7,400 h was initiated automatically due to progressive failures of the cells adjacent to short-circuited cell #8, which led to increasing leakages between the fuel and air sides of the stack and excessive temperatures, both in the stack and at the exhaust pipeline due to the burning of the fuel. This was seen as a catastrophic failure of the stack.

Additionally, between 2,500 and 3,500 h recurring difficulties related to the control of the inlet cathode air flow caused a steady increase in the inlet air flow, which manifests as a decrease of U_{AIR} in Figure 2. As a result of increased inlet air, the stack was cooled down progressively and the temperature and voltage of the stack were decreased. This decrease in voltage is seen as a decrease in $P_{el,stack}$ in Figure 2, as the stack was used with constant current density. The problem was solved by reconfiguring the control loop for cathode air, and thus a steady supply of air was restored.

Polarisation of the 5 kW stack was measured with hydrogen immediately after assembly and curing. After the curing and evaluation of stack performance with hydrogen, the unit and the stack were cooled down to ambient temperature for inspection and heated back to operating temperature to commence the experiments. Individual cell voltages of the stack with hydrogen at current density of 0.25 A cm^{-2} are depicted in Figure 3. Additionally, individual cell voltages measured during the experiment with reformed natural gas at 0.35 A cm^{-2} are shown for comparison. The distribution of individual cell voltages is identical with hydrogen and reformate gas i.e. the initial thermal cycle did not cause changes in the voltage distribution. Voltage of the cell #1 (bottom cell) was 50–100 mV lower compared to the other cells, and short-circuit was measured in the cell #8. The other cell voltages were within ±25 mV and similar values have been reported previously for FZJ stacks [23]. A slight increase in the voltage is observed towards the top of the stack, which is probably caused by the heating effect of the furnace, and due to the heat loss through the ceramic bricks at the bottom of the furnace. The differences between individual cell voltages, which are more pronounced in the middle of the stack (cells 20–30),

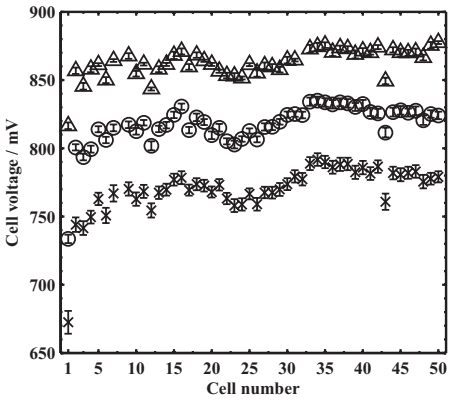

Fig. 3 Unit cell voltages of the stack at △ : hydrogen, U_{FUEL} = 0.6, j = 0.25 A cm^{-2}; ○ : natural gas, U_{FUEL} = 0.51, j = 0.35 A cm^{-2}; × : natural gas, U_{FUEL} = 0.71, j = 0.35 A cm^{-2}. Cell number 1 is located at the bottom of the stack. Error bars represent 2σ error.

can be due to differing contact resistances caused by inhomogeneous settling of the stack during the stack assembly and curing.

I–V curves of the stack with reformed natural gas at U_{FUEL} of 51% and 71% are depicted in Figure 4. After each current step, the system was left to stabilise for at least 24 h to reach new system-wide steady-state conditions i.e. so that no changes in the temperature measurements were observed. The time between the two different *I–V* curves depicted in Figure 4 is ~250 hundred hours. Electric power of 5.1 kW with U_{FUEL} of 51% was achieved at 0.35 A cm^{-2}. However, the $\eta_{el,stack}$ was only 33–35% due to low fuel utilisation level of the stack and also due to high inlet air O_2/C -ratio to the reformer, as part of the natural gas was oxidised already in

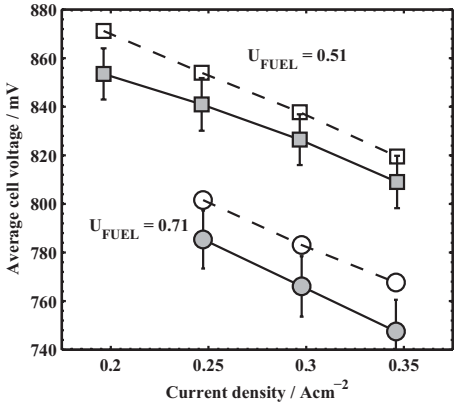

Fig. 4 Average unit cell voltage of the stack *versus* current density where U_{FUEL} is ○ = 0.71 and □ = 0.51. Fuel is pre-reformed natural gas. Solid line and filled marker: actual values measured from the stack. Dashed line and open marker: averaged values without cell #8. Error bars represent 2σ error.

the reformer reactor (see Section 3.2). The efficiency was improved by higher fuel utilisation and lower inlet air O_2/C ratios, as relatively larger fraction of the inlet fuel was used to produce electricity. With U_{FUEL} of 71%, electric power of 4.7 kW was achieved and the $\eta_{el,stack}$ was increased to ~48%. The short-circuited cell caused a decrease in the performance of the stack by lowering the stack voltage up to 2.5% during the *I–V* measurements. However, despite the performance loss, the robustness of the stack design towards short-circuits was demonstrated as stable operation was maintained up to 6,000 h during the experiment.

Performance degradation of varying magnitude was observed in the stack throughout the experiment. The measurements from the 5 kW stack were compared to the inherent voltage degradation of stacks with similar design and materials. The performance degradation of SOFC stacks is typically measured by operating the stack galvanostatically at constant operating conditions for several thousands of hours. The degradation can then be calculated from the absolute [$\Delta U \Delta t^{-1}$ (mV kh^{-1})] or relative [$\Delta U U_1^{-1} \Delta t^{-1}$ (%kh^{-1})] voltage drop over time and the resulting value can be used to express the durability of the stack. As the demonstration unit and the stack were used in varying operating conditions throughout the experiment, it is impossible to calculate any single value for stack voltage drop for the entire duration of the test based on the above described practice. Instead, the degradation of the stack is evaluated here by observing the evolution of absolute voltage drop of the stack voltage over time.

The average cell voltage of the stack during the experiment is depicted in Figure 5a. The absolute voltage drop is calculated with linear regression for all periods at steady-state operating conditions over 100 h. Measurements from the short-circuited cell (#8) are not used in the linear regression, as this generates step transitions in the voltage, which would produce misleading values for linear regression. Additionally to the steady-state conditions, the voltage drop is calculated with linear regression between periods where operation at identical conditions was resumed. The time periods and operating conditions used to calculate the absolute voltage drop, along with the results of linear regression are summarised in Table 1.

The resulting values for absolute voltage drop over time are depicted in Figure 5b. The absolute voltage drop was 20–135 mV kh^{-1} during the first 400 h of operating conditions and the voltage drop gets smaller over time. After the initial 400 h, the voltage drop settles at 6–12 mV kh^{-1}. After 4,000 h, the result suggests that the voltage drop is again increasing. Comparable values of absolute voltage drop over time for similar first generation (1-G) F-design short stacks have been reported by de Haart et al [5]. With 1-G short stacks, the initial voltage drop was 100–135 mV kh^{-1} during the first 300 h, which corresponds to the values obtained in the demonstration unit. Concurrently, after the initial drop in voltage, a linear decrease in voltage was measured over time. The linear decrease of voltage for 1-G short stacks was 6 mV kh^{-1} at 0.3 A cm^{-2}, and 16 mV kh^{-1} at 0.4 A cm^{-2}, which again corre-

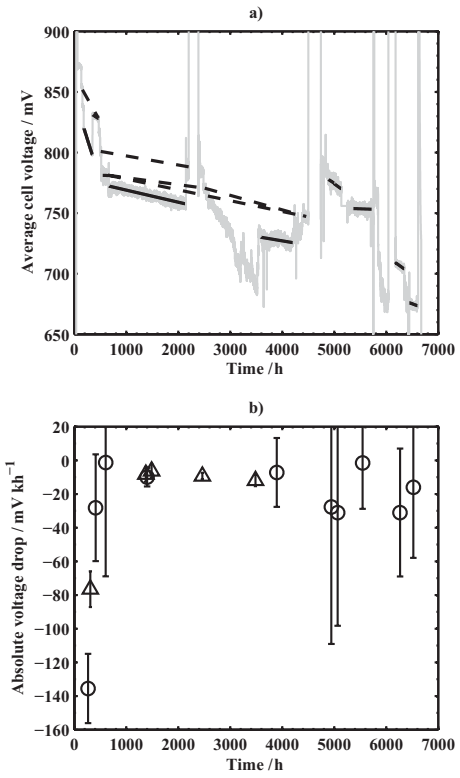

Fig. 5 Evolution of the stack voltage during experiment. a) Average cell voltage of the stack over time without cell #8 (grey line), linear fit for voltage at steady-state operating conditions (black solid line) and linear fit between identical operating conditions (black dashed line). b) Voltage decrease obtained with linear fitting at steady-state operating conditions (○) and between identical operating conditions (△). Error bars represent 2σ error in linear fit.

Table 1 Time period and operating conditions where the absolute voltage drop over time is calculated with linear regression. Error estimate for linear regression that meets 2σ variance in voltage measurements.

t_1	t_2	j	U_{FUEL}	U_{AIR}	Inlet O_2/C	Operating	ΔU	ΔU 2σ error
Hours		A cm^{-2}				Conditions	mV kh^{-1}	mV kh^{-1}
185	345	0.35	0.51	0.35	0.25	Steady-state	–136	21
156	462	0.25	0.51	0.38	0.30	Identical	–77	11
355	465	0.25	0.51	0.37	0.35	Steady-state	–28	32
545	660	0.30	0.71	0.37	0.10	Steady-state	–1	68
670	2 130	0.35	0.71	0.36	0.10	Steady-state	–10	6
510	2 428	0.25	0.71	0.38	0.19	Identical	–8	4
650	2 509	0.30	0.71	0.38	0.10	Identical	–6	4
650	4 460	0.30	0.71	0.37	0.10	Identical	–9	2
2 509	4 460	0.30	0.71	0.38	0.10	Identical	–12	3
3 590	4 200	0.35	0.71	0.26	0.00	Steady-state	–7	20
4 890	5 000	0.20	0.71	0.64	0.00	Steady-state	–28	81
5 000	5 130	0.20	0.71	0.68	0.00	Steady-state	–31	67
5 370	5 720	0.25	0.71	0.49	0.00	Steady-state	–2	27
6 190	6 345	0.20	0.71	0.59	0.20	Steady-state	–31	38
6 445	6 600	0.20	0.70	0.54	0.20	Steady-state	–16	42

spond to the values between 1,000 and 4,000 h of operation presented in Figure 5b. When the 1-G short stacks were used at current a density of 0.4 A cm^{-2} or higher, the voltage drop started to increase progressively before 3,000 h of operation. This progressive degradation was observed to increase towards higher current densities. After 4,000 h, the stack in the demonstration unit exhibits signs of progressive voltage decrease as well. However, relatively large error margin for the absolute voltage drop, due to measurement noise and short period of constant operation conditions, prevents obtaining a reliable value for the magnitude of progression. Nevertheless, both the magnitude and the different periods in the evolution of the absolute voltage drop over time correspond well between the 5 kW stack and similar 1-G stacks. Therefore, it can be concluded that the voltage degradation of the stack is inherent to the stack design itself i.e. no distinct increase in the degradation is observed due to choice of BoP-components, materials and design or system operating conditions.

3.2 Performance and Durability of BoP-components

The performance of the BoP-components used in the demonstration unit was suffcient to obtain the designed electrical output for the stack with gross electric efficiency of 45–50%. Fuel processing unit, air and fuel heat exchangers and the automation system worked as designed and performed reliably during the test run. The performances of the afterburner and power conversion unit were sub-optimal, but did not impede the performance of the stack.

The fuel reformer used in the demonstration unit provided means to control the degree of pre-reforming of the natural gas by varying the inlet air O_2/C-ratio and the H_2O/C-ratio [22]. By increasing the inlet air O_2/C-ratio, the faradic equivalent current efficiency of the reformer is lowered [24], as the part of the inlet fuel reacts with oxygen *via* partial oxidation reactions (Eq. 1).

$$\eta_{far} = \left(1 - 0.5 \times \frac{O_2}{C}\right) \quad (1)$$

In order to minimise the risk of carbon formation in the reactor, fuel pipelines and stack, the H_2O/C-ratio was increased as the O_2/C-ratio was decreased. The minimum H_2O/C-ratio in relation to O_2/C-ratio was selected to exhibit no graphite formation at thermodynamic equilibrium above 350 °C, and was defined according to Equation 2.

$$\frac{H_2O}{C} = 1.44 \times \left(\frac{O_2}{C}\right)^2 - 2.88 \times \frac{O_2}{C} + 2 \quad (2)$$

The effect of varying inlet air O_2/C-ratio to the outlet temperature (position

f6, Figure 1) of the reactor and on the gas composition of the reactor exhaust gas is depicted in Figure 6. The temperature at the reactor inlet (position f5) varied between 530 and 550 °C. At steam reforming mode (O_2/C ratio = 0), the *DoR* of methane in the natural gas was ~10%, and the *DoR* of ethane and propane was above 97% while the rest of the higher hydrocarbons in the natural gas were below detection limit. It should be noted that the *DoR* was nearly proportional to the inlet O_2/C-ratio and at O_2/C-ratio of 0.4 the degree of pre-reforming was increased to 90%. Concurrently, η_{far} decreased from 100% at steam reforming mode to 80% at O_2/C-ratio of 0.4.

The experimental results of the reformer characterisation were compared to the thermodynamic equilibrium at corresponding conditions. The equilibrium temperature and the composition of the reformate gas was calculated with Cantera toolbox [25] using GRI-Mech 3.0 reactions developed for natural gas combustion [26]. Equilibrium was solved for an adiabatic system, where the total enthalpy and pressure between reactants and products were kept constant. Temperature measurement at the reactor inlet (Figure 6) and measurements from mass flow controllers were used to define inlet gas mixture temperature and composition.

The experimental values are within the error limits when compared to the corresponding equilibrium values, except at O_2/C -ratios below 0.1 (Figure 6). At O_2/C -ratios below 0.1 the measured outlet temperature methane concentration are higher with respect to the equilibrium values. This deviation can be due to the catalyst kinetics, which limit the extent of the endothermic steam reforming reactions, as both the methane concentration and temperature at the outlet are higher than the corresponding equilibrium values.

Ageing of a natural gas pre-reformer catalyst can be assessed by observing the change in the methane conversion over time [27]. Decrease in the catalyst activity towards conversion of methane with an adiabatic reactor would show as decrease in the *DoR* and increase in the reactor outlet temperature, as less methane is consumed by endothermic steam reforming reactions. The long-term performance of the catalyst with respect to *DoR* and reactor outlet temperature is depicted in Figure 7. Again, both experimental and equilib-

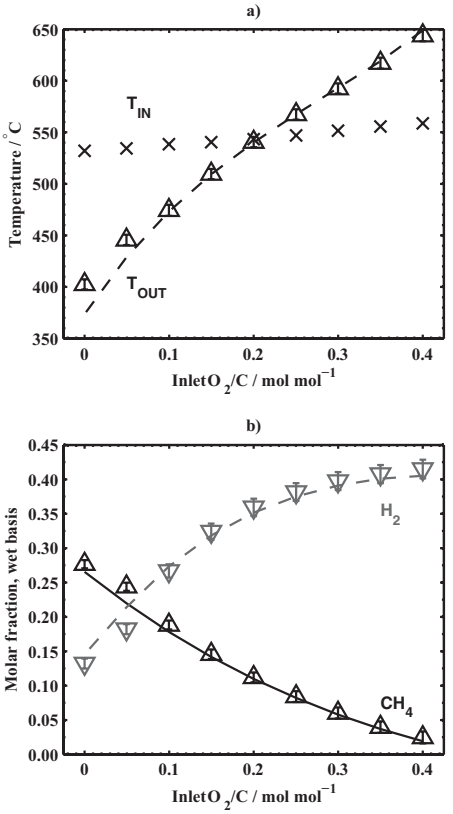

Fig. 6 Inlet O_2/C-ratio *versus* a) x = temperature at the reactor inlet and △ = temperature at the reactor outlet and b) ▽ = molar fraction of hydrogen and △ = molar fraction of methane. Markers represent the measured values and lines the equilibrium values.

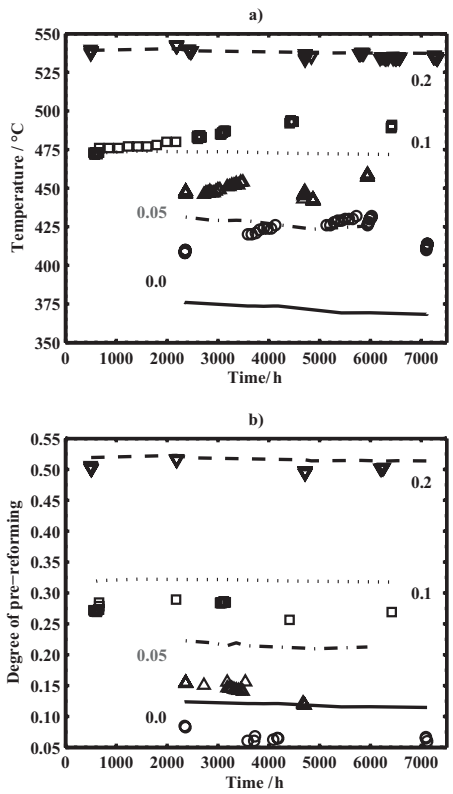

Fig. 7 a) Temperature at the reactor outlet and b) degree of pre-reforming gas during the test run with varying inlet air O_2/C -ratio. Markers represent the measured values and lines equilibrium values. Inlet air O_2/C -ratio was 0.0 (○, solid line), 0.05 (△, dash-dot), 0.1 (□, dotted) and 0.2 (▽, dashed).

rium results are presented. The performance can be evaluated with several inlet O_2/C -ratios as the demo unit was used at varying conditions. With inlet O_2/C -ratio of 0.2, no changes in either the temperature or the *DoR* can be seen over time. With lower O_2/C -ratios, the difference in the reactor outlet temperature increases by a maximum of 25 °C as the experiment proceeds further when compared to equilibrium values. A similar effect can be perceived with *DoR*, but the effect is not so pronounced as with temperature. These results indicate that some deactivation of the catalyst occurred, as the extent of steam reforming reactions decreased during the test run. Moreover, the deactivation can be more pronounced towards lower O_2/C -ratios, where larger portion of the methane is converted *via* steam reforming instead of partial oxidation reactions. However, the changes in the temperature are within 25 °C and the corresponding change in the *DoR* is only a few percent units. It can be argued that a deactivation of this magnitude is not an issue in the system operation, as the heat balance of the system is not significantly changed.

The characteristic performance of the air heat exchanger bundle is depicted in Figure 8a. It can be seen that the inlet air (position a3) was preheated to 530–580 °C and the temperature was increasing with the inlet air flow. The conductance of the heat exchanger bundle was 28.5 W K^{-1} and 79 W K^{-1} with 200 l_N min^{-1} and 600 l_N min^{-1}, respectively. The conductance increased linearly as a function of air flow rate. The relative decrease in temperature at lower air flow rates is due to considerable heat losses from the air exhaust pipeline between the stack and the heat exchangers, and from the heat exchanger bundle itself. Heat loss was calculated to be 13–15% from the hot air flow in the heat exchangers and 6–12% in the stack exhaust pipeline, depending on the air flow rate (data not shown). The temperature difference between the air flows at the stack end of the heat exchanger bundle remained at 150 ± 10 °C, regardless of the variation in the inlet air flow rate and the temperature of the hot air from the stack.

The characteristic performance of the air heat exchanger bundle remained constant during the test run. Figure 8b depicts the difference between temperature measurements at the stack end and blower end of the heat exchanger bundle. It is clear that the temperature difference remains at the above mentioned 150 ± 10 °C over time with some fluctuations caused by system stand-by situations. This indicates that the heat-transfer properties of the heat exchangers remain unchanged during the experiment. Likewise, no changes in the characteristic pressure drop at the hot side and the cold side of the HEX bundle were measured (data not shown).

No changes in the pressure losses at the fuel heat exchanger were observed over time. The pressure loss at each side of the fuel exchanger and in the fuel side of the stack was 5–20 mbar depending on inlet fuel flow rate, degree of pre-reforming and fuel utilisation of the stack. The pressure loss of the reformer reactor was below 5 mbar, while the vaporiser and fuel heater contributed 40–100 mbar to the total backpressure of the fuel system. The total backpressure of the components at the fuel system remained below 200 mbar

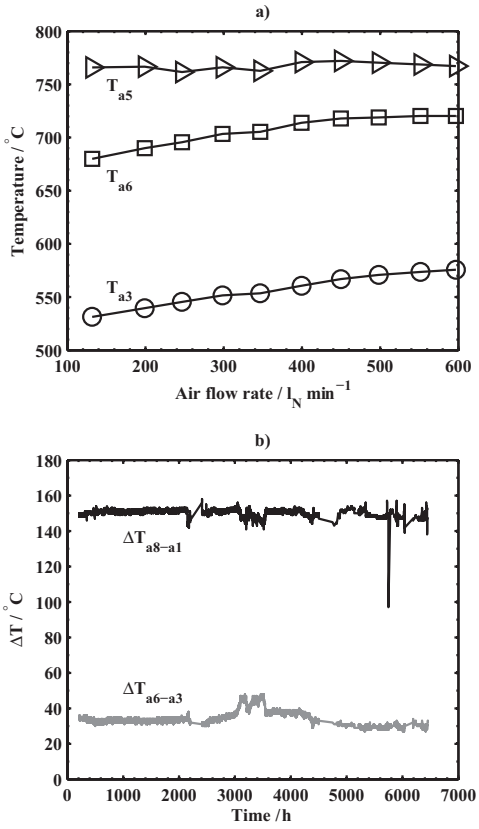

Fig. 8 Operation of the heat exchangers at the air system. a) Temperature of the air at the fresh side outlet of the HEX (▷), hot side inlet of the HEX (○) and at the stack exhaust (□). b) Temperature difference the inlet and out-let gases at the hot end and cold end of the HEX bundle, respectively. Current density was 0.2–0.35 A cm^{-2} during the measurements.

during the experiment. The heat transfer properties of the fuel heat exchanger cannot be evaluated reliably as the trace heating elements inflicted bias to the temperature measurements of the fuel and exhaust gases. Additionally, the vicinity of the air heat exchanger of considerably larger mass may have caused bias in the measurements as the heat exchangers were insulated under the same insulation layer. However, the heat exchanger operated through the entire test run and provided sufficient pre-heating of inlet fuel to operate the unit.

In atmospheric SOFC systems, the air blower is typically largest consumer of electric power among all auxiliary components [19]. Therefore, the characteristic backpressure of a SOFC system largely defines the parasitic power losses and the resulting decrease in the electric efficiency. The backpressure at different measurement positions at the air system *versus* the inlet air flow, along with the calculated power consumption of the air blower, are depicted in Figure 9. The power consumption of the air blower as a function of the air flow rate is calculated with fan efficiency of 25% and the total

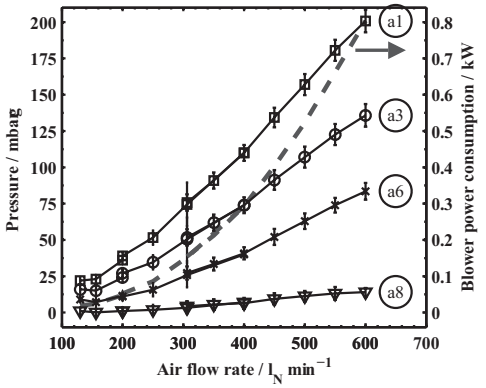

Fig. 9 Pressure at different measurement positions at air system (solid line and markers) and the power consumption of the blower (dashed line). Current density was 0.25–0.35 A cm^{-2} during the measurements. Error bars represent 2σ error.

backpressure of the system (a1, Figure 1). Constant total efficiency (electricity to pV-work) was assumed for the entire operating range of the blower. The power consumption of the blower is calculated to be 300 W at 400 l_N min^{-1}, which corresponds 26% of U_{AIR} at a current density of 0.35 A cm^{-2}. With $P_{el,stack}$ of 4.5–5 kW, the power consumption of the blower is below 10% of the gross stack electric power, and the decrease in the $\eta_{el,stack}$ is below 3%-units. The pressure loss of each component at the air system contributes to the total backpressure. With 400 l_N min^{-1}, the individual pressure losses of the hot and cold side of the heat exchanger bundle, and the stack are ~30 mbar. With this backpressure, the use of regular side-channel blowers is feasible as the parasitic power losses caused by the air blower remain below 300 W and the resulting decrease in the electrical efficiency is kept at an adequate level.

Two BoP -components, the power conversion unit and the afterburner, failed to operate as expected. The SOFC stack was connected to the electric grid with a power conversion unit whenever electric load was applied during the test run. A current setpoint was imposed on the power conversion unit, which limited the current density of the stack to the desired value. However, at maximum, half of the electricity produced by the stack could be supplied to the grid as the power conversion equipment caused an increasing voltage ripple on the stack at higher current levels. Therefore, the stack was loaded in parallel with the DC load to limit the current to the power conversion unit and to obtain high enough current densities for the test.

Cabling losses were 5–10%, calculated as loss of voltage between the stack end plates and the power conversion unit, and redesign of the current collection and cabling is required to decrease the losses. The conversion efficiency from DC input to AC output of the power conversion unit was ~70% with 2.5 kW input power. DC–DC converters that increased the DC voltage of the stack to 400 VDC for the inverter were the primary cause for the poor efficiency, having efficiency of ~80%. The low efficiency of the power conversion unit is partly explained by the use of regular off-the-shelf components that were not optimised for the low voltage and high current output of the stack. Significant improvements in the power conversion unit can be expected by utilising customised components.

Shortly after the stack assembly and system start-up, the burner failed to ignite and burn the anode off-gas from the stack. The failure was probably caused by condensation of liquid water to the surface of the catalysts during commissioning of the stack and the first thermal cycle. The condensed water rinsed away the catalytically active material, and no oxidation of fuel could occur in the afterburner. Prior to the long term testing, the afterburner was characterised in a separate test bench [24] and an endurance test of 1,000 h was conducted before assembling the burner to the demo unit. During the endurance test the burner showed no measurable decrease in performance. In the future experiments, a more robust afterburning catalyst tolerant to water condensation is needed or the condensation has to be prevented by redesigning the burner.

4 Conclusion

A SOFC demonstration unit was designed and constructed. The unit was operated with a planar SOFC stack for a total of over 7,000 h. During the test run the performance and durability of the stack and other BoP-components were assessed. Two components, the afterburner and the power conversion unit failed to operate as intended, but the performance of other components was satisfactory during the test run. The SOFC stack used in the system showed stable operation for long term testing and towards several shutdown situations, even with one cell in short-circuit.

The heat exchanger bundle at the air system operated with sufficient effectiveness to pre-heat the inlet air for stack operation. The total pressure losses at the air system were low enough to make use of regular side channel blowers feasible. At the fuel system, the combined effect of high heat loss and the use of trace heating prevented the assessing of the effectiveness of the heat exchanger. Nevertheless, the fuel heat exchanger was used successfully throughout the experiment and no distinct changes in the pressure loss or stack inlet temperature at the fuel side were observed. The operational characteristics of the reformer unit are assessed by comparison with thermodynamic equilibrium. A minor decrease in the DoR of the reformer was measured during the test run, but the change is not significant for system operation and was not observed to impede the performance of the stack.

The evolution of the voltage drop of the 5 kW power class stack used during the test run corresponds with the measurements conducted with similar short stacks. A period of large initial drop in voltage, followed by a period of nearly con-

stant voltage drop, is evident in the experimental results. Moreover, both the magnitude and time scale of these two phenomena match with the short stack experiments. It can, therefore, be concluded that the different system components, e.g. reformer or heat exchangers upstream of the stack, and varying operating conditions during the test run, did not cause a measurable increase in the inherent voltage degradation of the stack.

Acknowledgements

The authors would like to thank Wärtsilä Oyj, Automation Technology Laboratory of Helsinki University of Technology and Verteco Inc. for participating in the designing of the 5 kW SOFC unit. Forschunzentrum Jülich is gratefully acknowledged for providing and assembling the stacks for the unit. Dr L.G.J. (Bert) de Haart is acknowledged for his valuable input on operational issues with the stack. Mr. Reinhard Erben is thanked for his involvement in the stack assembly and instrumentation. Mr. Kari Koskela and Mr. Jorma Stick are specially acknowledged for their valuable effort in the construction of the unit. Funding for this study was obtained from FINSOFC and SofcPower projects. Finnish Funding Agency for Technology and Innovation in Finland (TEKES) as well as the companies that participated in the projects are gratefully acknowledged for their financial support.

List of Symbols

j	current density, A cm^{-2}
I_{stack}	total current of the stack, A
$P_{el,stack}$	gross DC electric power of the stack, $U_{stack}I_{stack}$, W
$\eta_{el,stack}$	gross DC electric efficiency of the stack, $\frac{P_{el,stack}}{\dot{n}_{NG}\Delta H_{NG,LHV}}$
$\Delta H_{NG,LHV}$	lower heating value for natural gas in Finland, 805.68 kJ mol^{-1}
T	temperature, °C
U	voltage, V
$\dot{n}$	molar flow rate, mol s^{-1}
NTP	normal temperature (0 °C) and pressure (101,325 Pa)
F	Faradys's constant (96,485 C mol^{-1})
G	conductance of a heat exchanger $\frac{\dot{n}(h_{cold,out}-h_{cold,in})}{\Delta T_{ln}}$, W K^{-1}
ΔT_{ln}	logarithmic mean temperature difference for a counter-flow heat exchanger $\frac{(T_{hot,out}-T_{cold,in})-(T_{hot,in}-T_{cold,out})}{\ln((T_{hot,out}-T_{cold,in})/(T_{hot,in}T_{cold,out}))}$, K
h	specific enthalpy or enthalpy increment, W mol^{-1} K^{-1}
U_{AIR}	air utilisation of the stack, $\frac{I_{stack}}{0.21\dot{n}_{AIR}4F}$
U_{FUEL}	fuel utilisation of the stack
Inlet O_2/C	air oxygen to fuel carbon ratio at the reformer inlet
Inlet H_2O/C	water to fuel carbon ratio at the reformer inlet
DoR	degree of pre-reforming of methane of the reformer $\frac{\dot{n}^{in}_{CH_4}-\dot{n}^{out}_{CH_4}}{\dot{n}^{in}_{CH_4}}$
σ	standard deviation

References

[1] L. Blum, H-P Buchkremer, R. W. Steinbrech, B. De Haart, Uwe Reisgen, R. Steinberger-Wilckens, Current Trends of SOFC Development at Forschungzentrum Juelich, Proc. 8th European SOFC Forum, Conference CD, **2008**, File No. B0306.

[2] E. Fontell, T. Kivisaari, N. Christiansen, J.-B. Hansen, J. Pålsson, *J. Power Sources* **2004**, *131*, 49.

[3] Y. Kayahara, M. Yoshida, Residential CHP Program by Osaka Gas Company and KYOCERA Corporation, *Proc. 8th European SOFC Forum*, Conference CD, **2008**, File No. B0304.

[4] N. Christiansen, J. B. Hansen, H. Holm-Larsen, M. Joergensen, L. T. Kuhn, P. V. Hendriksen, A. H. S. Linderoth, Solid Oxide Fuel Cell Research and Development at Topsoe Fuel cell A/S and Risoe/DTU, *Proc. 8th European SOFC Forum*, Conference CD, **2008**, File No. B0304.

[5] L. G. J. de Haart, J. Mougin, O. Posdziech, J. Kiviaho, N. H. Menzler, Stack Degradation in Dependence of Operation Parameters the Real-SOFC Sensitivity Analysis, Fuel Cells, **2009**, *9*, 794.

[6] E. Fontell, T. Hottinen, T. Lehtinen, Progress of the Wärtsilä Fuel Cell Program, *Proc. 8th European SOFC Forum*, Conference CD, **2008**, File No. B0406.

[7] T. Hottinen, T. Lehtinen, J. Hansen, E. Fontell, Operational Experiences from Wärtsilä 5 kW Test System with 4 SOFC Stacks, *Proc. 2nd European Fuel Cell Technology and Applications Conference*, **2007**, pp. 45–46 (EFC2007–39026).

[8] R. A. George, *J. Power Sources* **2000**, *86*, 131.

[9] S. Mukerjee, K. Haltiner, R. Kerr, L. Chick, V. Sprenkle, K. Meinhardt, C. Lu, Y. Kim, S. Weil, *ECS Trans.* **2007**, *7*, 59.

[10] J. Kiviaho, M. Halinen, M. Noponen, J. Saarinen, Finnish Platform for SOFC Research and Development, Fuel Cell Seminar 30, Conference CD, **2006**.

[11] A. Gubner, J. Saarinen, J. Ylijoki, D. Froning, A. Kind, M. Halinen, M. Noponen, J. Kiviaho, Dynamic Co-Simulation of Solid Oxide Fuel Cell (SOFC) and Balance of Plant (BoP) by Combining an SOFC Model with the

BoP-Modelling tool APROS, Proc. 7th European SOFC Forum, Conference CD, **2006**, File No. B092.
[12] T. Ollikainen, J. Saarinen, M. Halinen, T. Hottinen, M. Noponen, E. Fontell, J. Kiviaho, *ECS Trans.* **2007**, *7*, 1821.
[13] J. Saarinen, M. Halinen, A. Gubner, M. Noponen, J. Ylijoki, A. Kind, J. Kiviaho, Steady-State Simulation Study of Thermal Management of Planar SOFC Stack, Fuel Cell Seminar 30, Conference CD, **2006**.
[14] I. Vinke, R. Erben, R.-H. Song, J. Kiviaho, Installation and Operation of kW-Class Stacks from Jülich in External Laboratories, *Proc. 7th European SOFC Forum, Conference CD*, **2006**, File No. B036.
[15] R. Steinberger-Wilckens, I. C. Vinke, L. Blum, L. B. de Haart, J. Remmel, F. Tietz, W. Quadakkers, Progress in Stack Development at Forschungzentum Jülich, *Proc. 6th European SOFC Forum* **2004**, *1*, 11.
[16] J. J. Hartvigsen, S. Elangovan, A. Khandkar, System design, in: *Handbook of Fuel Cells Fundamentals, Technology and Applications, Vol. 4*, **2003**, pp. 1071–1085, ISBN: 0-471-49926-9.
[17] N. Dekker, J. Outweltjes, G. Rietveld, *ECS Trans.* **2007**, 7, pp. 1465.
[18] H. Timmermann, W. Sawady, D. Campbell, A. Weber, R. Reimert, E. Ivers-Tiffé, *J. Electrochem. Soc.* **2008**, *155*, B354.
[19] E. Riensche, U. Stimming, G. Unverzagt, *J. Power Sources* **1998**, *73*, 251.
[20] M. Noponen, M. Halinen, J. Kiviaho, J. Saarinen, *J. Fuel Cell Sci. Tech.* **2006**, *3*, 444.
[21] M. Noponen, M. Halinen, J. Saarinen, J. Kiviaho, *ECS Trans.* **2007**, *5*, 545.
[22] M. Halinen, M. Noponen, J. Saarinen, J. Kiviaho, Characterization and Control of a Autothermal Reformer for SOFC Applications, Fuel Cell Seminar 30, Conference CD, **2006**.
[23] L. Blum, H.-P. Buchkremer, S. Gross, A. Gubner, L. B. deHaart, H. Nabielek, W. Quadakkers, U. Reisgen, M. J. Smith, R. Steinberger-Wilckens, R. Steinbrech, F. Tietz, I. Vinke, **2007**, Fuel Cells 3, pp. 204–210.
[24] J. Saarinen, M. Halinen, J. Ylijoki, M. Noponen, P. Simell, J. Kiviaho, *J. Fuel Cell Sci. Tech.* **2007**, *4*, 397.
[25] D. Goodwin, An open-source, extensible software suite for cvd process simulation, Proceedings of CVD XVI and EuroCVD 14, The Electrochemical Society PV 2003-2008, **2003**, pp. 155–162, see also http://www.cantera.org/.
[26] G. Smith, GRI-MECH 3.0, http://www.me.berkeley.edu/gri_mech/.
[27] R. Peters, E. Riensche, P. Cremer, *J. Power Sources* **2000**, *86*, 432.

